

In vivo anticancer efficacy assessment with an imaging-based platform: taking Brucea Javanica oil emulsion as an example

Ye-Wei Liu^{1,2}, Ting Yin¹, Yuan-Bo Feng¹, Feng Chen¹, Jie Yu¹, Jian-Jun Liu², Shao-Li Song², Uwe Himmelreich¹, Raymond Oyen¹, Gang Huang^{2,3,4}, Yi-Cheng Ni¹

¹Department of Imaging and Pathology, Faculty of Medicine, Katholieke Universiteit Leuven, 3000 Leuven, Belgium.

²Institute of Clinical Nuclear Medicine, Renji Hospital, Shanghai Jiao Tong University School of Medicine, Shanghai 200127, China.

³Institute of Health Sciences, Shanghai Jiao Tong University School of Medicine (SJTUSM) & Shanghai Institutes for Biological Sciences (SIBS), Chinese Academy of Sciences (CAS), Shanghai 200025, China.

⁴Shanghai University of Medicine and Health Sciences, Shanghai 201318, China.

Correspondence to: ¹Dr. Yi-Cheng Ni, Theragnostic Laboratory, Department of Imaging and Pathology, Faculty of Medicine, Katholieke Universiteit Leuven, Herestraat 49, 3000 Leuven, Belgium. Email: yicheng.ni@med.kuleuven.be

²Dr. Gang Huang, Institute of Clinical Nuclear Medicine, Renji Hospital, Shanghai Jiao Tong University School of Medicine, Shanghai 200127, China. Email: huang2802@163.com

How to cite this article: Liu YW, Yin T, Feng YB, Chen F, Yu J, Liu JJ, Song SL, Himmelreich U, Oyen R, Huang G, Ni YC. *In vivo* anticancer efficacy assessment with an imaging-based platform: taking Brucea Javanica oil emulsion as an example. *J Unexplored Med Data* 2016;1:21-9.

Article history:

Received: 01-07-2016

Accepted: 29-07-2016

Published: 13-09-2016

Key words:

Brucea Javanica oil emulsion, rat R1 rhabdomyosarcoma, magnetic resonance imaging, angiography, therapeutic response

ABSTRACT

Aim: Brucea Javanica oil emulsion (BJOE) has already been commercialized to treat various malignancies. The authors verified BJOE for its therapeutic effects on rhabdomyosarcoma (R1) in rats using magnetic resonance imaging (MRI), microangiography and histopathology. **Methods:** Rats were implanted with R1 in both flanks and subjected to intratumoral injections of BJOE or normal saline on day 0 and 7 for intra-individual comparisons. Therapeutic responses were compared between treated and control tumors at a 3.0 T MRI on day 0, 7 and 14 using T2-, T1-, and diffusion-weighted imaging that generated apparent diffusion coefficient (ADC) with b values of 0, 50, 100, 150, 400, 600, 800 and 1,000 s/mm². Volumes of necrotic and viable tumors were measured and verified with histopathology and tumor vascularity was quantified on microangiography. **Results:** After BJOE administration, tumor growth slowed down with increased intratumoral necrosis ($P < 0.05$) and reduced tumoral blood flow ($P < 0.05$). ADC maps differentiated viable and necrotic tumor components. Microangiography and histopathology supported MRI findings. **Conclusion:** Local BJOE injection created necrosis, reduced the growth and lowered vessel density in rat R1 tumors. MRI allowed monitoring tumor growth and quantifying therapeutic responses. As a non-invasive and contrast-agent-free technique, ADC maps helped distinguish the necrotic from viable tumor tissues.



This is an open access article distributed under the terms of the Creative Commons Attribution-NonCommercial-ShareAlike 3.0 License, which allows others to remix, tweak, and build upon the work non-commercially, as long as the author is credited and the new creations are licensed under the identical terms.

Quick Response Code:



For reprints contact: service@oaepublish.com



INTRODUCTION

Brucea javanica (BJ) is a traditional Chinese herbal medicine [Figure 1A and B] that has been originally used to treat various ailments like amebic dysentery and malaria. In China, as a commercial therapeutic product [Figure 1C], BJ oil emulsion (BJOE) has been commercialized to treat various malignancies including lung cancer, digestive tract cancers, prostate cancer and cervical cancer as well as their metastases.^[1] Research indicated that BJ exerts its anti-cancer effect by the active components^[2-6] [Figure 1D] in its seeds including quassinoids,^[7-10] triterpenoids,^[11-13] flavonolignan and flavonoids,^[11,12,14] pregnane glycosides^[6,9] and oleic and linoleic acid,^[6] etc. and mainly via the activation of caspase-dependent mitochondrial apoptotic pathway, and P53-, NF-kappa B-, COX-2-dependent death receptor pathways.^[15-20]

The formulations of BJ extracts has been largely improved aiming at raising anti-cancer activity and lowering toxicity of each single formula, while the anti-cancer effects in numerous human cancer cell lines have been constantly remarkable. The aqueous extract of BJ has been identified to exhibit cytotoxic effects in A549 non-small cell lung cancer, Hep3B hepatocellular carcinoma, methane dicarboxylic aldehyde-MB231 breast cancer, SLMT-1 esophageal squamous cell carcinoma,^[16] and PANC-1, SW1990, CAPAN-1 pancreatic adenocarcinoma.^[17,18] Also, BJ oil (BJO) was proven to induce apoptosis of T24 bladder cancer cells.^[19] Encouragingly, the successful preparation of BJOE allowed the *in vivo* evaluation of anti-cancer effect of BJ.^[15,21] For the acute myeloid leukemia, BJOE has been shown to interfere molecular signaling pathways in U937 and Hodgkin lymphoma-60 cell lines as well as primary acute myelocytic leukemia patients' leukemic cells, but not in normal peripheral blood lymphocytes.

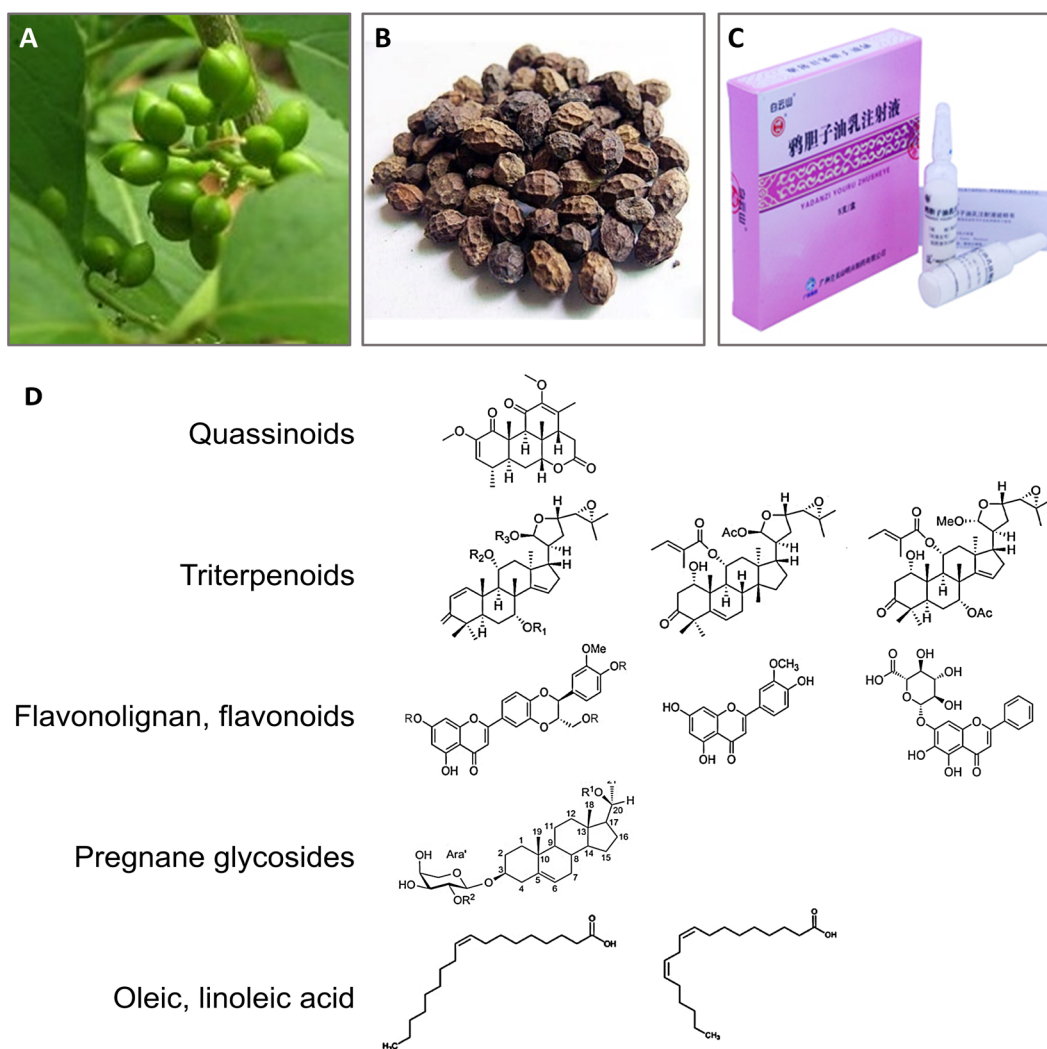


Figure 1: Plant (A) and dry fruits (B) of Brucea Javanica and its oil emulsion as a parenteral injectable medicine (C). Basic chemical structures of anti-cancer compounds extracted from Brucea Javanica (D).

Such anti-leukemia effects of BJOE were further verified *in vivo* in U937 leukemia xenograft in nude mice by BJOE intravenous injection.^[15] Positive *in vivo* results were also shown in the S-180 sarcoma-bearing mice by intravenous administration of a mixture containing of BJO and coix seed oil.^[21]

Nevertheless, the therapeutic effects of BJOE on rodent solid malignancies such as rhabdomyosarcoma remain unexplored particularly in terms of noninvasive imaging therapeutic monitoring. To this end, we first generated a rat model of bifocal subcutaneous engrafts of rhabdomyosarcoma-1 (R1). Therapeutic effects of BJOE were compared intra-individually using normal saline (NS) as blank control in the rats with R1 tumors, and evaluated by noninvasive magnetic resonance imaging (MRI) as *in vivo* imaging biomarker and verified by *ex vivo* microangiography and histopathology.

METHODS

Reagents and cell line

The commercial BJOE [Figure 1C] was obtained from Mingxing Pharmaceutical Co. Ltd. (Guangzhou, China). Rat R1 cell line was kindly provided by Dr. P. Schoffski, Dr. A. Wozniak and J. Wellens (Laboratory of experimental oncology, Department of oncology, KU Leuven).

Rat model of R1 subcutaneous rhabdomyosarcoma allograft

All *in vivo* procedures including tumor implantation, drug injection and imaging were performed under gas-anesthesia with 2% isoflurane in the mixture of 20% oxygen and 80% room air using a gas-anesthesia system (Harvard apparatus, Holliston, MA). Thirteen wistar albino glaxo (WAG)/Rij rats weighting around 250 g were recruited for the experiments. Initially, R1 cells (2×10^6) suspended in 200 μ L phosphate buffer solution were injected into the dorsal subcutaneous tissue of a donor rat. Three weeks later, tumor derived from R1 cells was harvested from the donor, cut into 1 mm³ blocks, and implanted bilaterally into the right and left flank regions of the recipient rats. The donor rats were then euthanized. Tumor growth was followed by MRI weekly from the third week after implantation.

Experimental design

The experiments started when the tumor diameters reached ≥ 1.0 cm at day 21 post implantation. These rats were intratumorally injected with BJOE at a dose of 0.6 mL/kg body weight ($n = 12$) and NS solution ($n = 12$) respectively served as a control at each lateral on day 0 and 7. All rats were noninvasively examined by MRI on day 0, 7, 14. Rats were euthanized after the last time point of MRI for postmortem microangiography and

histopathology [Figure 2]. Therapeutic responses were compared intra-individually between tumors of both sides and inter-individually among tumors at different time points.

In vivo MRI

MRI was performed on a clinical 3.0T whole body magnetic resonance magnet (Trio, Siemens, Erlangen, Germany) with a human wrist coil (MRI Devices, Waukesha, WI) on day 0, 7 and 14. The rats were placed supinely in a plastic holder inside the coil.

After the acquisition of scout images for localization, axial and coronal T2-weighted (repetition time, 4,320 ms; echo time, 69 ms; flip angle, 150°; field of view, 75 \times 56.25 mm²; matrix, 512 \times 384; slice thickness, 3.0 mm) and T1-weighted (repetition time, 500 ms; echo time, 39 ms; flip angle, 160°; field of view, 75 \times 56.25 mm²; matrix, 512 \times 384; slice thickness, 3.0 mm) turbo spin echo multislice imaging (T2WI, T1WI), and axial diffusion-weighted (repetition time, 3,500 ms; echo time, 102 ms; field of view, 117 \times 87.75 mm²; matrix, 96 \times 72; slice thickness, 3.0 mm) imaging (DWI) with a spin-echo-type echo-planer imaging sequence were performed *in vivo*. Diffusion gradients were applied in 3 dimensions (x, y and z) with 8 different b values of 0, 50, 100, 150, 400, 600, 800 and 1,000 s/mm², and averaged for calculating the isotropic apparent diffusion coefficient (ADC) values.

MRI analyses

Image analysis was conducted using the built-in software on the Siemens workstation (version Numaris/4 Syngo MR A30) and ImageJ software (version 1.47, NIH, Bethesda, MD, USA) to obtain the following measurables. All measurements were acquired by 3 authors with consensus.

Tumor volume

On T2WI, tumor area was manually contoured with an operator-defined region of interest on all tumor-containing images. The total tumor volume (mm³) was calculated by using the following equation: tumor volume = \sum [tumor area on each slice \times (slice thickness + gap)].

Intratumoral necrosis ratio

Central area with a relatively higher intensity on T2WI and a high intensity on ADC maps is considered necrosis. The tumor area and the necrotic area were quantified by manually delineating the tumor mass covering the whole tumor and the necrosis inside tumor on each T2WI slice, respectively. The necrosis ratio was calculated by the following formula: necrosis ratio (%) = \sum [necrotic area on each slice \times (slice thickness + gap)] / \sum [tumor area on each slice \times (slice thickness + gap)] \times 100.

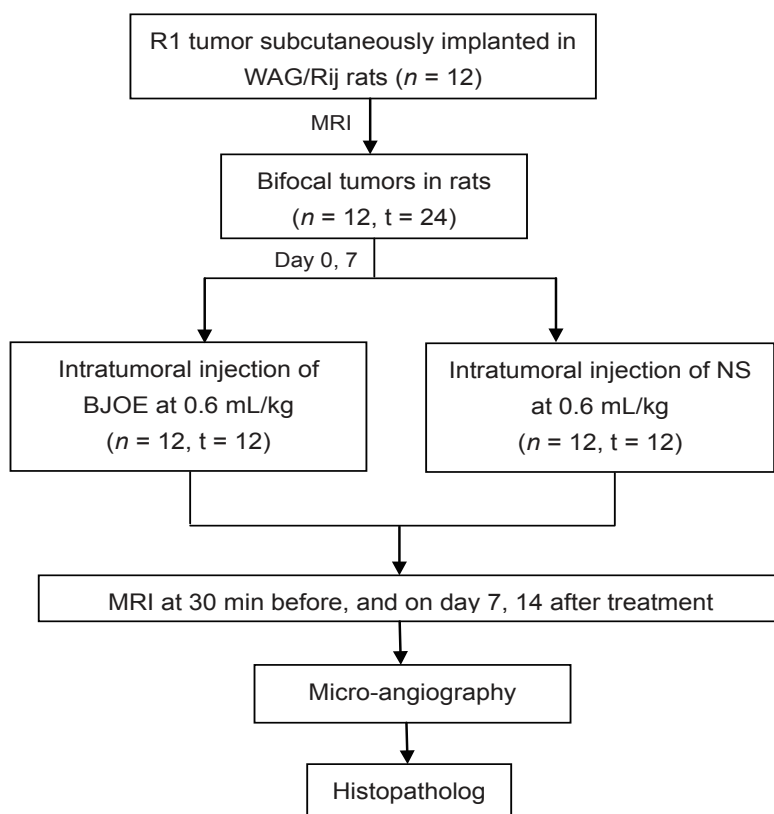


Figure 2: Flow chat of experimental design. R1: rhabdomyosarcoma-1; n: number of animals; t: number of tumors; MRI: magnetic resonance imaging; BJOE: Brucea Javanica oil emulsion; NS: normal saline

Viab le tumor ratio

The peripheral area with a relatively lower intensity on T2WI and ADC maps is considered viable tumor tissue. The viable tumor ratio was calculated using the following equation: viable tumor ratio (%) = $\sum [(tumor\ area\ on\ each\ slice - necrotic\ area\ on\ each\ slice) \times (slice\ thickness + gap)] / \sum [tumor\ area\ on\ each\ slice \times (slice\ thickness + gap)] \times 100$.

Separate calculation of tumor ADC

ADC maps were calculated from DWI to quantify therapeutic responses by the following mono-exponential formula: $S_i = S_0 \times \exp(-b_i \times ADC)$, in which S_i is the signal intensity (SI) measured on the i th b value image, b_i is the corresponding b value, and S_0 is a variable estimating the intrinsic SI (for $b = 0\ s/mm^2$).

For the calculation of different ADC values, viable tumor tissue was firstly freehand delineated on all slices of the original DWI at the b value of $1,000\ s/mm^2$. The delineations of each tumor lesion were merged and form one 3D volume of interest, which was copied to all images with different b values automatically. The average SI per tumor and per b value was then determined. The difference between ADC_{low} ($b = 0, 50$ and $100\ s/mm^2$) and ADC_{high} ($b = 600, 800$ and $1,000\ s/mm^2$) was defined as ADC_{perf} to reflect the tissue microcapillary perfusion.

Imaging software MeVisLab (version 2.6.2, MeVis Medical Solutions AG, Bremen, Germany) was used to perform the delineations and calculations.^[22]

Digital microangiography and vessel density quantification

After the last time point of MRI scanning, rats were anesthetized by an intraperitoneal injection of pentobarbital (Nembutal; Sanofi Sante Animale, Brussels, Belgium) at $50\ mg/kg$, and heparinized by an intravenous bolus injection of heparin (Leo Pharma AB, Malmö, Sweden) at $500\ U/kg$ via the penial vein. From a cervical incision, the right carotid artery was retrogradely catheterized, and the arterial blood was collected by a 10 mL syringe. Barium sulfate suspension (Micropaque®, Guerbet, France) was then injected gradually via the carotid catheter at the volumes of 1, 2, 3, 4, 5 mL, while the rats were stepwise radiographed with a digital mammography unit (Embrace; Agfa-Gevaert, Mortsel, Belgium) at 26 kV, 32 mAs. Afterwards, all tumors were excised and radiographed again by the same digital mammography unit. The tumors were then fixed and sliced into 3mm sections in the axial plane corresponding to the MRI using a plexiglas matrix (Agar Scientific, England), and these sections were radiographed at 26 kV, 18 mAs for quantification of vessel density.

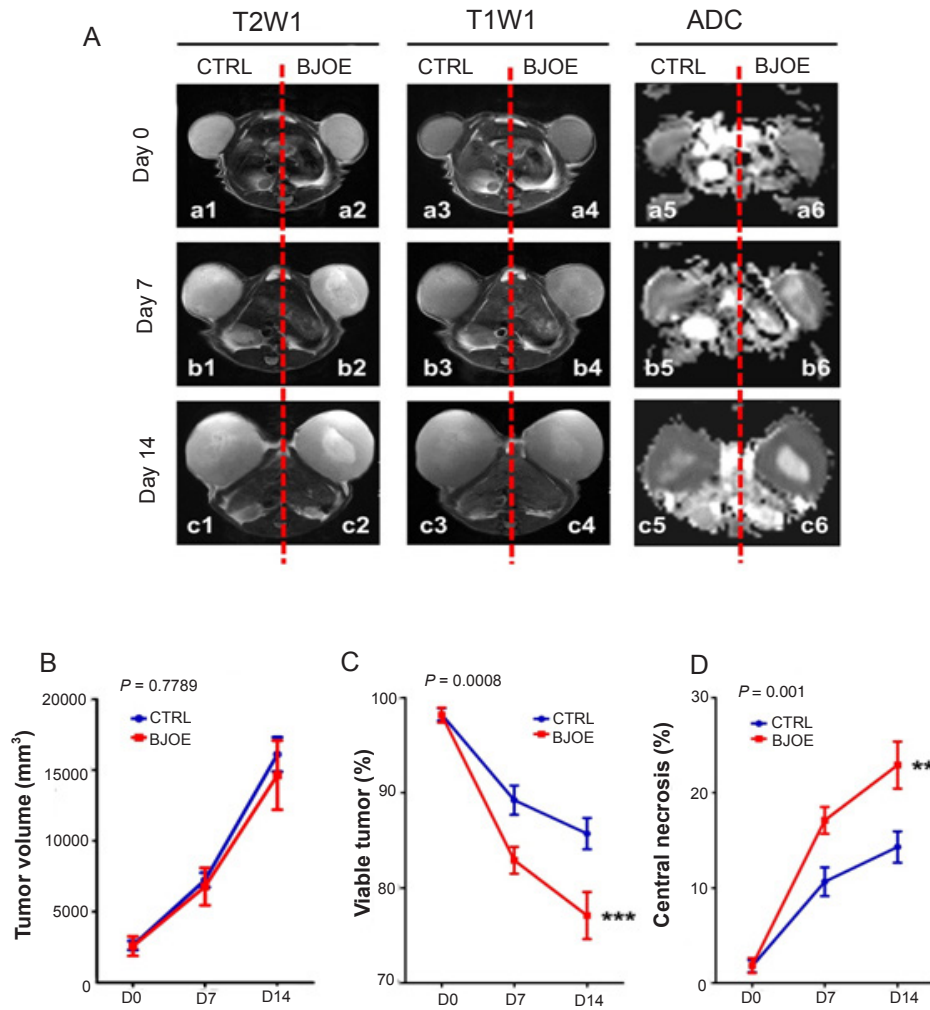


Figure 3: Representative MRI findings in a R1 tumor-bearing rat on day 0 baseline, and day 7 and 14 post BJOE and NS treatments (A). Tumors treated with both BJOE and NS appear hyperintense on T2WIs, and nearly isointense on T1WIs; intratumoral necrosis appeared highly hyperintense as a central core. On ADC maps, bilateral tumors share the same signal intensity at baseline on day 0, suggesting the intact tumor viability; however, tumors showed stronger signals in the center on day 7 and 14 after BJOE and NS injections, suggesting spontaneous and therapeutic tumor necrosis, respectively. Tumor growth curve (B), and corresponding viable tumor (C) and intratumoral necrosis (D) ratios between BJOE treated (red line, $n = 12$) and control (blue line, $n = 12$) groups on day 0 baseline, and day 7 and 14 post treatment measured from T2WI. No significant difference was found in tumor volume between the two groups. Intratumoral necrosis in BJOE treated group was found significantly raised than that in control group from day 7 on; meanwhile, viable tumor significantly decreased after BJOE treatment. Results are means \pm SEM. ** $P < 0.01$, *** $P < 0.001$. MRI: Magnetic resonance imaging; BJOE: Brucea Javanica oil emulsion; NS: normal saline; ADC: apparent diffusion coefficient; SEM: standard error of the mean

Digital photographs from microangiography were analyzed for quantification of relative vessel density using ImageJ. Briefly, the light background was first subtracted from each photograph by the 20 pixels of rolling ball radius. The tumor area was manually selected and mean gray value, as an index of the intratumoral vessel density, was then measured. The generated mean gray values were compared between the BJOE and saline treated tumors.

Hematoxylin and eosin staining and histopathology

After microangiography, the tumor sections were paraffin imbedded, sliced into 5 μ m thickness and stained with hematoxylin and eosin for microscopic analysis using an Axiovert 200 M microscope equipped with an AxioCam MR

monochrome digital camera (Carl Zeiss Inc, Gottingen, Germany) at 50 \times to 200 \times magnification. AxioVision 4.8 software was used. Histological findings were further cross-validated with the corresponding *in vivo* MRI and postmortem microangiographic images.

Statistical analysis

Numerical data were presented as mean \pm standard errors of the mean. Results between the BJOE treated tumors and the corresponding control tumors were compared by two-way ANOVA in combination with Bonferroni post-test using the GraphPad Prism (version 5.01, GraphPad Software Inc, La Jolla, CA, USA).

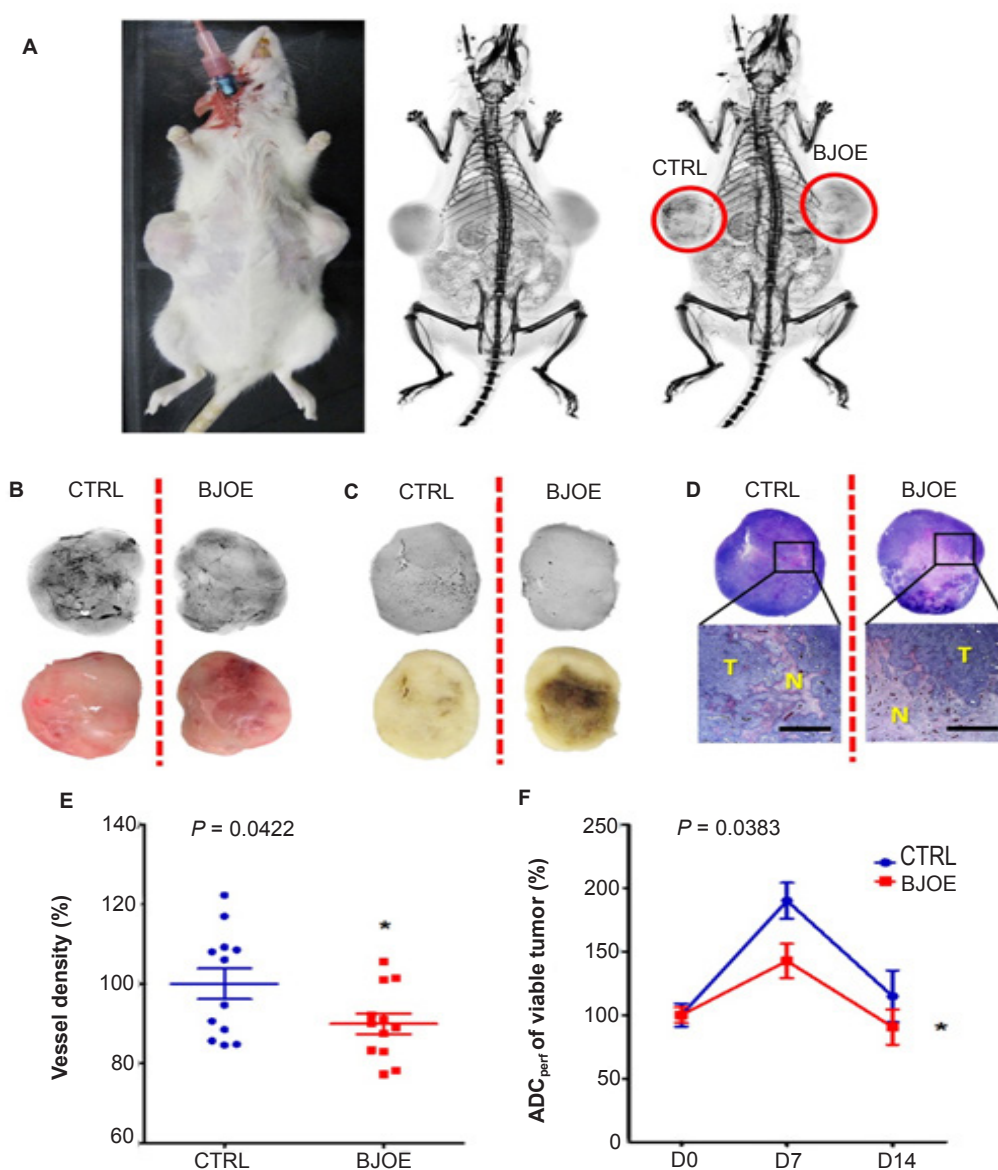


Figure 4: Anti-tumor angiogenesis effect of BJOE on rat R1 xenograft model. Gross postmortem photograph (left), digital radiograph of whole-body projection (middle) and microangiogram after systemic perfusion with 4 mL barium sulfate via carotid artery (right) of R1 tumor-bearing rat on day 14 post the first treatment (A). Microangiograms (upper panels) and macrographs (lower panels) for entire tumors (B). Representative tumor tissue blocks of 3 mm thickness (C) indicating that tumor angiogenesis of BJOE treated group was sparser than that of control group by intra-individual comparison. Macroscopic photographs (upper panels) confirmed the spontaneous necrosis in control tumor (left) and the treatment-induced necrosis in BJOE treated tumor (right) surrounded by viable tumoral tissues; rectangular frames denote the area where microscopy was focused (D). Microscopically (lower panels), the interface between necrotic (N) and viable (T) tumor tissues were confirmed (HE staining, $\times 12.5$ original magnification, scale bar = 1 mm). Quantification of *ex vivo* microangiogram-derived tumor vessel density (E) depicting significantly reduced tumor vessel density in BJOE treated tumors ($n = 12$) compared with control tumors ($n = 12$) on day 14. $*P < 0.05$ by two-tailed unpaired *t*-test. ADC_{perf} (F) decreased after BJOE treatment on day 7 and 14. $*P < 0.05$ by two-way ANOVA analysis. BJOE: Brucea Javanica oil emulsion; ADC: apparent diffusion coefficient

RESULTS

General condition

All rats survived the entire experimental procedures including anesthesia, tumor implantation/growth and MRI sessions, and tolerated well intratumoral drug injection. The bifocal subcutaneous R1 tumor model was successfully established in all 12 rats, resulting in the sample size of 12

R1 tumors in each treatment group.

Weekly BJOE administration increased intratumoral necrosis and slowed down tumor growth in R1 allograft model in WAG/Rij rats

At baseline, both BJOE and NS treated tumors were hyperintense on T2WI [Figure 3Aa1, a2] and mildly

hyperintense on T1WI [Figure 3Aa3, a4], respectively. Seven days after BJOE [Figure 3Ab2, b4] and NS [Figure 3Ab1, b3] administrations, inhomogeneous hyperintense signals appeared in the central region of tumors on both T2WI and T1WI, indicating spontaneous and therapeutic tumor necrosis occurred. Fourteen days after treatment, a larger area of central necrosis was seen on the BJOE treated tumor [Figure 3Ac2, c4] compared with the NS treated tumor [Figure 3Ac1, c3].

On DWI-derived ADC maps, relative to homogeneous signal intensities in tumors on day 0 baseline [Figure 3Aa5, a6], BJOE treated tumors revealed more hyperintense and larger central regions on day 7 and 14 post treatment [Figure 3Ab6, c6] in comparison with NS treated tumors [Figure 3Ab5, c5], suggesting the enhanced water diffusion due to the central necrosis caused by treatment. In spite of the imaging distortion and artifact, ADC maps displayed a better contrast between the viable and necrotic tissues.

Quantitatively, the mean volume of tumors, and corresponding viable tumor and intratumoral necrosis ratio measured on T2WI indicated that BJOE administration only slightly slowed tumor growth [Figure 3B], but significantly decreased percentile viable tumor volume [Figure 3C] and increased the percentile tumor necrosis [Figure 3D] ($P < 0.01$).

Angiogenesis inhibition as an anticancer effect with BJOE

Stepwise systemic arterial infusion of barium sulfate suspension indicated areduced tumoral vascularization level in BJOE treated tumors compared with the NS treated tumors [Figure 4A]. Accordingly, digital microangiography showed that BJOE treatment caused sparser blood vessels both on the harvested entire tumors [Figure 4B] and on sliced tumor blocks [Figure 4C], relative to NS treated tumors, suggesting that BJOE increased intratumoral necrosis and reduced tumor angiogenesis, which was in line with *in vivo* MRI findings and supported by histopathological outcomes [Figure 4D].

Tumor vessel density derived from *ex vivo* microangiography was $100 \pm 13.35\%$ and $89.96 \pm 10.04\%$ in NS and BJOE treated tumors, respectively [Figure 4E], while ADC_{perf} from *in vivo* MRI showed a reduction of blood perfusion by 47.44% on day 7 and 24.22% on day 14 in viable tumors treated by BJOE compared to those treated by NS [Figure 4F]. These results suggested BJOE injection reduced tumoral vasculature in R1 allografts-bearing rats.

DISCUSSION

Utilizing natural products to develop potential new drugs for managing human diseases has been particularly

encouraged by the 2015's Nobel Prize in physiology and medicine.^[23] In this study, we reported, for the first time, that BJOE intratumoral injection significantly increased tumor necrosis and slowed down the growth of rhabdomyosarcoma allografts in rats, which evaluated by *in vivo* MRI, and verified by *ex vivo* radiography and histopathology. Moreover, by using *in vivo* DWI and *ex vivo* digital microangiography, angiogenesis inhibition was observed, which is likely involved in the anti-cancer effects of BJOE.

As a versatile method to noninvasively evaluate therapeutic effects in malignancies,^[24-26] MRI was used in our study, which allowed *in vivo* tumor growth monitoring and quantitative comparison of therapeutic responses of R1 tumors in rats. Moreover, ADC map derived from DWI, as a non-invasive and contrast-agent-free technique,^[22,27] helped distinguish the necrotic from viable tumor tissues sensitively, while ADC_{perf} as an imaging biomarker for blood perfusion, provided more information about tumor angiogenesis. Therefore, by intention, we did not apply contrast enhanced MRI to avoid any possible drug interference in therapeutic evaluation.

The anti-cancer effect of BJOE observed in R1 allograft model is in line with the previous *in vitro* results that BJO induced apoptosis at low concentrations and necrosis at higher concentrations selectively in various cancer cell lines.^[15,20] In this study, since we adopted intratumoral injection as the administration route, central tumoral tissue was treated in a relatively higher BJOE concentration leading to enlarged central necrosis, while the surrounding tumor tissue was affected in a relatively lower concentration or through an indirect way, which collectively may have caused tumor cell necrosis and slowed down tumor growth. Additionally, the intratumorally injected BJOE might positively affect also the contralateral tumors via absorption to the blood.

Besides, continuous BJOE treatment seems to improve therapeutic response effectively, as the tumor volume and percentile viable tumor dropped further after the second time of BJOE treatment in comparison with the period after the first treatment. This suggested that BJOE could be suitable for chronic treatment and can be administered intravenously in patients. In our further research, we would try the intravenous administration of BJOE instead at a relative higher frequency in R1 tumor-bearing rats and compare the therapeutic responses with intratumoral injection.

Angiogenesis is one of the main hallmarks of cancer,^[28] which plays critical role in tumor growth and spread. Neovascular targeting therapy is aiming at the abnormal morphology and functionality of the chaotic blood vessel network in the tumor. In our microangiographical

observations, a sparser vasculature appeared in BJOE treated tumors, suggesting angiogenesis inhibition was likely involved in the anti-cancer effects of BJOE, which was in line with the *in vivo* ADC_{perf} findings. Differing from the previously reported mechanism of BJ on malignancies^[15-20] by acting the caspase-dependent apoptotic pathway or through P53-, NF-kappa B-, COX-2-dependent death receptor pathways, anti-angiogenesis is mainly targeting endothelia of tumoral vessels or preventing tumoral vasculature, instead of direct effects on cancer cells. However, this possible novel anti-cancer effect of BJOE needs further verification in tumoral endothelial cells and in other tumor models.

Taken together, local BJOE injection created necrosis, reduced the growth and lowered vessel density in rat R1 tumors. MRI allowed monitoring tumor growth and quantifying therapeutic responses. As a non-invasive and contrast-agent-free technique, ADC map helped distinguish the necrotic from viable tumor tissues. On top of that, we have generated and applied a platform with rat model of R1 tumor allograft, with *in vivo* MRI diagnosis and post-mortem microangiography and histopathology evaluation, which might allow evaluating the anti-cancer effects of different other drugs as well.

Financial support and sponsorship

This work has partially been supported by KU Leuven projects IOF-HB/08/009 and IOF-HB/12/018, the KU Leuven Molecular Small Animal Imaging Center MoSAIC (KUL EF/05/08) and European Union (Asia-Link CfP 2006-EuropeAid/123738/ACT/Multi-Proposal No. 128-498/111); and by research grants from "973" Project (2012CB932604), New Drug Discovery Project (2012ZX09506-001-005), the National Natural Science Foundation of China (Grant No. 81530053, 81471685). Liu YW is sponsored by a scholarship from the center of excellence *in vivo* molecular imaging research (IMIR). The corresponding author is a Bayer Lecture Chair holder.

Conflicts of interest

There are no conflicts of interest.

Patient consent

No patient involved.

Ethics approval

All animal experiments were carried out in compliance with European and national regulations after approval from Katholieke Universiteit Leuven university ethics committee (P147/2013) for animal care and use.

REFERENCES

- Shan GY, Zhang S, Li GW, Chen YS, Liu XA, Wang JK. Clinical evaluation of oral fructus bruceae oil combined with radiotherapy for the treatment of esophageal cancer. *Chin J Integr Med* 2011;17:933-6.
- Lee K, Imakura Y, Sumida Y, Wu R, Hall I, Huang H. Antitumor agents. 33. Isolation and structural elucidation of bruceoside -A and -B, novel antileukemic quassinoid glycosides, and brucein -D and -E from Brucea javanica. *J Org Chem* 1979;44:2180-5.
- Ohnishi S, Fukamiya N, Okano M, Tagahara K, Lee KH. Bruceosides D, E, and F, three new cytotoxic quassinoid glucosides from Brucea javanica. *J Nat Prod* 1995;58:1032-8.
- Anderson MM, O'Neill MJ, Phillipson JD, Warhurst DC. *In vitro* cytotoxicity of a series of quassinoids from Brucea-javanica fruits against KB cells. *Planta Med* 1991;57:62-4.
- Zhao L, Li C, Zhang Y, Wen Q, Ren D. Phytochemical and biological activities of an anticancer plant medicine: Brucea Javanica. *Anticancer Agents Med Chem* 2014;14:440-58.
- Chen M, Chen R, Wang S, Tan W, Hu Y, Peng X, Wang Y. Chemical components, pharmacological properties, and nanoparticulate delivery systems of brucea javanica. *Int J Nanomedicine* 2013;8:85-92.
- Fukamiya N, Okano M, Miyamoto M, Tagahara K, Lee KH. Antitumor agents, 127. Bruceoside-C, a new cytotoxic quassinoid glucoside, and related-compounds from brucea javanica. *J Nat Prod* 1992;55:468-75.
- Kim IH, Hitotsuyanagi Y, Takeya K. Quassinoid xylosides, javanicosides G and H from seeds of Brucea javanica. *Heterocycles* 2004;63:691-7.
- Liu JQ, Wang CF, Li XY, Chen JC, Li Y, Qiu MH. One new pregnane glycoside from the seeds of cultivated brucea javanica. *Arch Pharm Res* 2011;34:1297-300.
- Liu JH, Zhao N, Zhang GJ, Yu SS, Wu LJ, Qu J, Ma SG, Chen XG, Zhang TQ, Bai J, Chen H, Fang ZF, Zhao F, Tang WB. Bioactive quassinoids from the seeds of brucea javanica. *J Nat Prod* 2012;75:683-8.
- Pan L, Chin YW, Chai HB, Ninh TN, Soejarto DD, Kinghorn AD. Bioactivity-guided isolation of cytotoxic constituents of brucea javanica collected in Vietnam. *Bioorg Med Chem* 2009;17:2219-24.
- Kim JA, Lau EK, Pan L, De Blanco EJ. NF-κB Inhibitors from Brucea javanica exhibiting intracellular effects on reactive oxygen species. *Anticancer Res* 2010;30:3295-300.
- Dong SH, Liu J, Ge YZ, Dong L, Xu CH, Ding J, Yue JM. Chemical constituents from Brucea javanica. *Phytochemistry* 2013;85:175-84.
- Chen Y, Angelova A, Angelov B, Drechsler M, Garamus VM, Willumeit-Römer R, Zou A. Sterically stabilized spongosomes for multi-drug delivery of anticancer nanomedicines. *J Mater Chem B* 2015;3:7734-44.
- Zhang H, Yang JY, Zhou F, Wang LH, Zhang W, Sha S, Wu CF. Seed oil of brucea javanica induces apoptotic death of acute myeloid leukemia cells via both the death receptors and the mitochondrial-related pathways. *Evid Based Complement Alternat Med* 2011;2011:e965016.
- Lau FY, Chui CH, Gambari R, Kok SH, Kan KL, Cheng GY, Wong RS, Teo IT, Cheng CH, Wan TS, Chan AS, Tang JC. Antiproliferative and apoptosis-inducing activity of Brucea javanica extract on human carcinoma cells. *Int J Mol Med* 2005;16:1157-62.
- Lau ST, Lin ZX, Zhao M, Leung PS. Brucea javanica fruit induces cytotoxicity and apoptosis in pancreatic adenocarcinoma cell lines. *Phytother Res* 2008;22:477-86.
- Zhao M, Lau ST, Leung PS, Che CT, Lin ZX. Seven Quassinoids from fructus bruceae with cytotoxic effects on pancreatic adenocarcinoma cell lines. *Phytother Res* 2011;25:1796-800.
- Lou GG, Yao HP, Xie LP. Brucea javanica oil induces apoptosis in T24 bladder cancer cells via upregulation of caspase-3, caspase-9, and inhibition of NF-kappa B and COX-2 Expressions. *Am J Chin Med* 2010;38:613-24.
- Gao H, Lamusta J, Zhang WF, Salmosen R, Liu Y, O'Connell E, Evans JE, Burstein S, Chen JJ. Tumor cell selective cytotoxicity and apoptosis induction by an herbal preparation from brucea javanica. *N Am J Med Sci (Boston)* 2011;4:62-66.
- Yu YL, Lu Y, Tang X, Cui FD. Formulation, preparation and evaluation of an intravenous emulsion containing brucea javanica oil and coix seed oil for anti-tumor application. *Biol Pharm Bull* 2008;31:673-80.

22. Chen F, De Keyzer F, Wang H, Vandecaveye V, Landuyt W, Bosmans H, Hermans R, Marchal G, Ni Y. Diffusion weighted imaging in small rodents using clinical MRI scanners. *Methods* 2007;43:12-20.
23. The Nobel Prize in Physiology or Medicine 2015[Internet]. [cited 2016 August 11]. Available from: http://www.nobelprize.org/nobel_prizes/medicine/laureates/2015/.
24. Wang H, Sun X, Chen F, De Keyzer F, Yu J, Landuyt W, Vandecaveye V, Peeters R, Bosmans H, Hermans R, Marchal G, Ni Y. Treatment of rodent liver tumor with combretastatin a4 phosphate: noninvasive therapeutic evaluation using multiparametric magnetic resonance imaging in correlation with microangiography and histology. *Invest Radiol* 2009;44:44-53.
25. Li J, Chen F, Feng Y, Cona MM, Yu J, Verbruggen A, Zhang J, Oyen R, Ni Y. Diverse responses to vascular disrupting agent combretastatin a4 phosphate: a comparative study in rats with hepatic and subcutaneous tumor allografts using MRI biomarkers, microangiography, and histopathology. *Transl Oncol* 2013;6:42-50.
26. Li J, Cona MM, Chen F, Feng Y, Zhou L, Yu J, Nuyts J, de Witte P, Zhang J, Himmelreich U, Verbruggen A, Ni Y. Exploring theranostic potentials of radioiodinated hypericin in rodent necrosis models. *Theranostics* 2012;2:1010-9.
27. Sun X, Wang H, Chen F, De Keyzer F, Yu J, Jiang Y, Feng Y, Li J, Marchal G, Ni Y. Diffusion-weighted MRI of hepatic tumor in rats: comparison between *in vivo* and postmortem imaging acquisitions. *J Magn Reson Imaging* 2009;29:621-8.
28. Hanahan D, Weinberg RA. Hallmarks of cancer: the next generation. *Cell* 2011;144:646-74.